METHODS PAPER

Neutron computed laminography yields 3D root system architecture and complements investigations of spatiotemporal rhizosphere patterns

Nicole Rudolph-Mohr [ID]· **Sarah Bereswill** [ID]·
Christian Tötzke [ID]· **Nikolay Kardjilov** [ID]·
Sascha E. Oswald [ID]

Abstract

Purpose Root growth, respiration, water uptake as well as root exudation induce biogeochemical patterns in the rhizosphere that can change dynamically over time. Our aim is to develop a method that provides complementary information on 3D root system architecture and biogeochemical gradients around the roots needed for the quantitative description of rhizosphere processes.

N. Rudolph-Mohr · S. Bereswill (✉) · C. Tötzke ·
S. E. Oswald
Institute of Environmental Science and Geography,
University of Potsdam, Karl-Liebknecht-Str. 24-25,
14476 Potsdam, Germany
e-mail: bereswill@uni-potsdam.de

N. Rudolph-Mohr
e-mail: nrudolph@uni-potsdam.de

C. Tötzke
e-mail: toetzke@uni-potsdam.de

S. E. Oswald
e-mail: sascha.oswald@uni-potsdam.de

N. Kardjilov
Institute of Applied Materials, Helmholtz-Zentrum Berlin
Für Materialien Und Energie, Berlin, Germany
e-mail: kardjilov@helmholtz-berlin.de

Methods We captured for the first time the root system architecture of maize plants grown in rectangular rhizotrons in 3D using neutron computed laminography (NCL). Simultaneously, we measured pH and oxygen concentration using fluorescent optodes and the 2D soil water distribution by means of neutron radiography. We co-registered the 3D laminography data with the 2D oxygen and pH maps to analyze the sensor signal as a function of the distance between the roots and the optode.

Results The 3D root system architecture was successfully segmented from the laminographic data. We found that exudation of roots in up to 2 mm distance to the pH optode induced patterns of local acidification or alkalization. Over time, oxygen gradients in the rhizosphere emerged for roots up to a distance of 7.5 mm.

Conclusion Neutron computed laminography allows for a three-dimensional investigation of root systems grown in laterally extended rhizotrons as the ones designed for 2D optode imaging studies. The 3D information on root position within the rhizotrons derived by NCL explained measured 2D oxygen and pH distribution. The presented new combination of 3D and 2D imaging methods facilitates systematical investigations of a wide range of dynamic processes in the rhizosphere.

🙋 Springer

Introduction

Plant-soil interactions induce a high spatiotemporal variability of soil properties in the root zone. Water and nutrient acquisition and the extent of biogeochemical gradients in the rhizosphere are connected to the spatial distribution of roots in soil and affected by the architecture of the root systems (Hinsinger et al. 2009, 2005; Smith and De Smeth 2012). Root respiration, water and nutrient uptake as well as root induced pH variations differ between roots of different physiological function, morphology and branching order (Ahmed et al. 2018; Rudolph-Mohr et al. 2017) as well as along single roots (Aguilar et al. 2003; Chaignon et al. 2002; Rudolph et al. 2013). Due to the highly variable nature of root growth, there is a clear need to gain complementary information about root system architecture and chemical composition of the rhizosphere over larger spatial and temporal scales, which has been identified as one of the key challenges in rhizosphere research (Roose et al. 2016).

In-situ imaging methods have been applied to study the root system of soil-grown plants. 3D non-invasive methods such as neutron tomography (Moradi et al. 2011; Tötzke et al. 2017, 2021), X-ray tomography (Aravena et al. 2011; Koebernick et al. 2017) or magnetic resonance tomography (Pohlmeier et al. 2008; van Dusschoten et al. 2016) can yield detailed information on root system architecture and rhizosphere behavior. The maximum diameter of the usually cylindrical plant containers ranges from 30–120 mm depending on the imaging modality as well as the desired spatial resolution. The temporal resolution depends on the time needed to perform the 3D scan and may range from seconds to hours (Tötzke et al. 2019). 2D imaging allows for studying larger root systems grown in slab-shaped rhizotrons with lateral dimensions of several hundred of millimeters. However, 2D approaches are intrinsically limited by averaging in transmission images such as neutron radiography (Menon et al. 2007; Moradi et al. 2009) or yield just a 2D imprint of the 3D root-soil compartment, as for example optical fluorescence imaging using planar optodes (Blossfeld et al. 2013; Rudolph-Mohr et al. 2017; Strömberg 2008). As each of the methods has specific strengths and limitations, the combination of

two or more techniques can provide complementary information on the root-soil system when applied simultaneously to the same sample. For instance, neutron tomography was recently combined with magnetic resonance imaging to achieve synergistic information of water mobility and total water content in the rhizosphere (Haber-Pohlmeier et al. 2019). Optical fluorescence imaging and neutron radiography are a unique combination to study plant root systems grown in slab-shaped rhizotrons in respect to dynamic changes (Rudolph-Mohr et al. 2014). The application of this combined imaging approach showed the dynamics of root respiration, pH changes and water uptake related to root morphology at high spatial and temporal resolution (Rudolph-Mohr et al. 2017). However, the interpretation of the observed 2D biogeochemical gradients had some ambiguity as the optical fluorescence sensors that were attached to the front or rear wall of the rhizotron capture the activity of roots in different distances with different contrast and timing. Therefore, extending this imaging set-up by a tomographic approach should be considered a crucial next step to link the biochemical information of soil with the 3D root system architecture (RSA).

Different requirements regarding sample size and geometry make the combination of 2D optical fluorescence imaging and 3D transmission tomography technically challenging. When it comes to measuring the three-dimensional RSA, a cylindrical shape of the plant container is a clear advantage as it ensures uniform transparency of the sample during the tomographic scan. The maximum possible diameter of such containers is limited to a few centimeters and depends on the actual attenuation property of the plant-soil sample. This imposes spatial constraints for root growth and thus limits the application of standard tomographic techniques to young plants. A slab-shaped rhizotron represents the optimum container design for 2D chemical imaging with planar optodes (Rudolph et al. 2012) allowing for studying root systems and water uptake on the scale of several decimeters in the lateral direction (Dara et al. 2015). However, the rectangular design has usually limited the imaging approach to two dimensions, since tomographic acquisition of the 3D root systems in such a container is associated with considerable difficulties. When the rhizotron is rotated during the tomographic scan, the large lateral extension of the container leads

to insufficient neutron transmission of the sample over a significant angular range. Although it is not impossible to perform standard neutron tomography of rectangular slabs (Esser et al. 2010), the image quality suffers from pronounced imaging artefacts due to the limited sector of accessible projection angles. An adapted tomographic technique especially suited for flat samples is computed laminography and it has been applied in synchrotron X-ray (Helfen et al. 2011b) and conventional X-ray CT-scanners (Fisher et al. 2019) as well as at neutron imaging instruments (Helfen et al. 2011a; Salvemini et al. 2015), but not yet with plant roots in soil. By tilting the rotational axis with respect to the incoming beam, each projection has a similar overall transmission over the full angular range of the scan, which is a better basis for a tomographic reconstruction.

The aim of the present study was to apply neutron computed laminography (NCL) for the first time to capture the RSA of maize plants grown in slab-shaped rhizotrons. This 3D information is useful by itself, but also required to enhance the interpretation of 2D pH and oxygen patterns captured by optical fluorescence imaging. Complementary neutron radiography was applied to obtain 2D water maps of the soil during the experiment. We co-registered the 3D laminography with the 2D fluorescence images to investigate to which extent the local root volume contributes to signal changes in the planar optodes. We hypothesize that also roots grown in some distance to the optode have an influence on the observed oxygen and pH values and therefore data on the entire root system is needed for a complete interpretation.

Material and methods

Plant growth

Three slab-shaped, boron-free glass rhizotrons (150 mm × 150 mm × 15 mm) were prepared with optodes either sensitive to pH or oxygen (covered area of 130 mm × 140 mm) glued to their inner sides. The rhizotrons were filled with quartz sand (grain size distribution 200–2000 μm, initial $pH_{(CaCl2)} = 6.57$) and separated into an upper and a lower compartment by a horizontal layer (width: 10 mm) of a fine sand-silt mixture (grain size distribution 1–250 μm).

As long as this layer was water saturated, it prevented gas exchange between the lower compartment and the ambient air allowing the observation of root oxygen consumption. The rhizotrons were covered with aluminum foil, which was only removed during the imaging procedure. Maize seeds (*Zea mays* L. cv. Golden Bantam) were germinated in the dark at 21 °C and planted two days after germination. The sand surface was covered with a 1 cm thick layer of coarse gravel to minimize evaporation. Plants were grown in a plant growth chamber (Vötsch, Balingen, Germany) with a daily photoperiod of 14 h with a light intensity of 300 μmol m^{-2} s^{-1}. The light intensity was ramped up from zero to 100% between 6 a.m. and 8 a.m. and ramped down between 6 p.m. and 8 p.m. Temperature was 25 °C during the day and 19 °C at night, the relative humidity was kept at 60%. Plants were irrigated with nutrient solution (as described in Rudolph-Mohr et al. 2017) during the growing period of 19 days. At the start of the experiment, the maize plants were 21 days old (calculated after sowing).

Neutron radiography and computed laminography

Neutron imaging enables the detection of roots and soil water content due to the sensitivity to hydrogen bearing materials. Neutron radiography is a two-dimensional transmission imaging technique able to map the RSA and changes in the local soil water content of the root-soil system in 2D. The soil water content θ was determined from the neutron radiographs according to the method described in Rudolph-Mohr et al., (2017). In the drier range ($\theta < 0.15$ cm^3 cm^{-3}), the volumetric soil water content is determined with approx. ± 5% accuracy. At higher soil moisture ($\theta > 0.15$ cm^3 cm^{-3}) scattering artefacts increase the relative error up to ± 10%. The pixel size of the neutron radiographs was 100 μm corresponding to a physical spatial resolution of approx. 200 μm. The root system of plants grown in slab-shaped rhizotrons mainly extends in vertical and lateral direction, which can be captured by 2D neutron radiography. However, the actual root system represents a 3D-structure where the third spatial direction (i.e. the thickness of the slab orientated in the direction of the propagating beam during radiographic measurements) contains the information about the distance of the roots to the planar optodes measuring pH and O$_2$. Extracting this

information requires a tomographic approach that can capture sample objects with large lateral extension. Computed laminography (Helfen et al. 2011a, b) is such an adapted tomographic approach. In standard tomography, the axis of sample rotation is orientated perpendicular to the beam. The basic idea of computed laminography is to tilt this axis, such that the sample transmission stays at a constant level for the full set of projections. This way, artefacts related to highly attenuated images that limit standard tomography can be eliminated or at least mitigated. We performed NCL on three maize plants at the neutron imaging instrument CONRAD-2 (BER II, Helmholtz Centre Berlin, Germany) (Kardjilov et al. 2016). Note that tilting the rotational axis in plant experiments bears the risk of mechanical changes in the soil and of bending the plant stem because the aboveground part of the plant may slide across the detector when rotated by full 360°. Yet, for a complete reconstruction of a tomographic scan, a full 360° is not necessarily required. To avoid any movement of roots and soil or even the loss of sand during the scan the rhizotrons were sealed at the top, and mounted on a sample holder in front of the detector (Fig. 1a). The rotational axis was then tilted by an angle of 20° (γ) towards the vertical. Since the sample was mounted lying on the rotation table holder the container plane had an angle of 70° to the detector plane and the vertical (Fig. 1b). The collimation ratio (L/D) was 330 limiting the geometrical blurring to ~400 μm, which was the limitation of the spatial resolution in this

experiment. The field of view in this experiment was 200×200 mm^2 and the voxel size was 99 μm. We captured 450 projections (exposure time: 30 s) over a 205° rotational range resulting in a scan time of 4 h per plant. The mean volumetric soil water content was 0.10 cm^3 cm^{-3} at the start of NCL.

Optical fluorescence imaging with planar optodes

Oxygen concentrations and pH values were measured using planar optodes. These optical sensors are thin foils in which a fluorescent dye is incorporated in a polymeric matrix. Setups for optical imaging rely on fluorescence emission that varies in intensity depending on the concentration of the analyte. The fluorescent sensors were manufactured and calibrated at University of Potsdam as described in Rudolph-Mohr et al. (2014). Changes in fluorescence intensity were captured using a cooled camera system (Kappa DX 4C-285 FW) with a 500 nm long-pass filter and a UV light (type 215 L, Peqlab, Erlangen, Germany). The field of view of the fluorescence images was 258 mm $\times$ 221 mm, resulting in a pixel size of 360 μm.

Experimental set-up

At the beginning of the experiment, the rhizotrons were wetted from the bottom until the soil reached field capacity referring to a mean volumetric water content of 0.24 cm^3 cm^{-3}. After this irrigation

Fig. 1 Setup for neutron computed laminography (NCL). **a** Test rhizotron filled with sandy soil and featuring an oxygen optode. The rhizotron is fixed in a sample holder and positioned in front of the neutron detector. The direction of the neutron beam path is indicated by the big red arrow. **b** The rotational stage with the maize sample is mounted on a goniometer to adjust the tilt angle versus the vertical; here the axis is tilted by 20° towards the detector
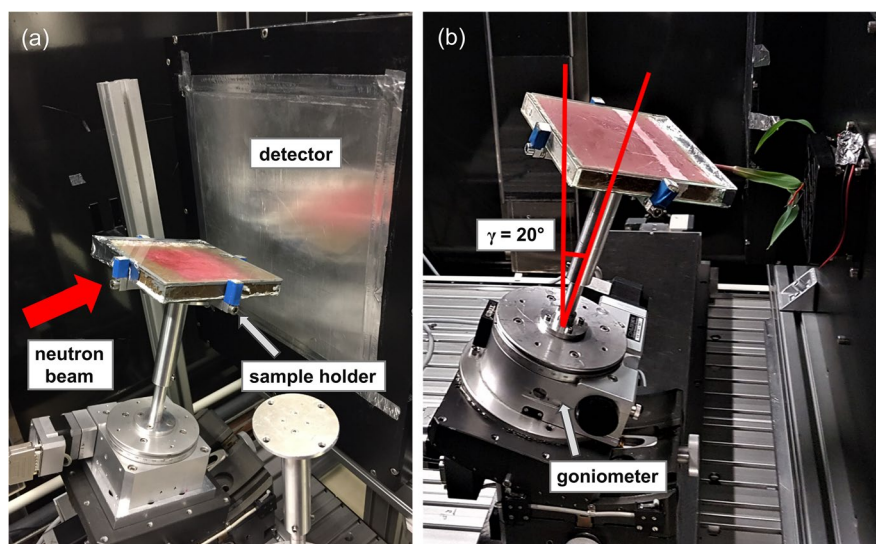
event, we took 2D neutron radiographs and fluorescence images simultaneously every 3 h in order to image root growth, soil water content as well as pH- and oxygen dynamics during the following 5 days. Between the measurements, the plants were kept in a plant growth chamber close to the neutron imaging instrument maintaining the light, temperature and humidity conditions the plants experienced during the growing period. After 5 days without further watering, we applied NCL to capture the 3D root system architecture.

Image processing and analysis

The projections from NCL were corrected for camera noise and beam fluctuations. Reconstruction of the 3D volume of the samples was performed with the software Octopus Reconstruction 8.9.4 (Inside Matters, Gent/Belgium; cone beam geometry, axis skew: 20°). The root system was segmented using the region growing algorithm implemented in VG Studio Max 3.1 (Volume Graphics, Heidelberg/Germany). Starting from a user-defined seed-point placed within a root, the region of interest is expanded in three dimensions. Voxels connected to the initial selection that do not deviate more than a defined tolerance value from the average gray value of the voxels within the growing region are added (dynamic mode). Placement of several initial seeds and local adjustment of the gray-scale value threshold was required to segment all visible roots. The segmented root system was skeletonized using the plugin 'Skeletonize3D' in Fiji (https://imagej.net/Skeletonize3D). For each slice of the 3D volume, the number of pixels belonging to the root skeleton was multiplied by the voxel size and divided by the slice volume to calculate the root length density distribution (RLD in $mm\ mm^{-3}$) within the rhizotron. Additionally, total root length was calculated separately for the upper and lower compartment (above resp. below the horizontal layer) by multiplying the total number of root pixels by the voxelsize. Co-registration of the fluorescence images and the reconstructed data from NCL was achieved by scaling the images and manually setting landmarks using the software ImageJ (https://imagej.net/). Oxygen concentrations and pH values were calculated from the gray-scale fluorescence images according to Rudolph-Mohr et al. (2014). The segmented 3D image of the root system was compartmented into 1 mm thick slices in the z-direction to illustrate the influence of the root-sensor distance on the O_2 and pH maps. The Euclidean distance transform was calculated from the segmented 3D root systems in Fiji (plugin 'Exact Euclidean Distance 3D') to plot oxygen concentration as a function of distance to the nearest root surface in the 3D domain.

Results

3D root system architecture

The three-dimensional structure of the root system of three maize plants grown in slab-shaped rhizotrons could be successfully reconstructed from the neutron computed laminography scans. The quality of the reconstructed 3D object showed to be appropriate to perform a semi-automated segmentation of the root system based on region growing algorithms. Figure 2 provides different perspective views on the segmented root system of an exemplary selected maize plant (sample 1). The front view (central panel of Fig. 2) resembles a 2D-view as obtained by neutron radiography, but offers also a visual perspective due to the third dimension. It shows the well-developed root system, which extends through the horizontal barrier layer shown as gray shadowed area. This layer was introduced to study root oxygen consumption under limited gas exchange with the ambient air in the lower compartment of the rhizotron. The considerably higher water content of the sand-silt material in the barrier layer made the segmentation of the roots more challenging. Due to unfavorable contrast, the segmentation algorithm missed to detect a few roots within this region. The laterally arranged panels of Fig. 2 show top and bottom view as well as the respective side views of the root system. It is evident that even in such a flat rhizotron, roots form a 3D structure and often several different roots overlap. In 2D neutron radiography, those roots cannot be distinguished from each other and neither their relative positioning and connections. It is clearly visible that roots tended to grow more along one side of the rhizotron, i.e. along the pH-sensor. The mean spatial distribution of the root length of the three maize individuals within the rhizotron shows that root length close to the front is higher than close to the back side or the center of the rhizotron, especially between z = 0–7.5 mm (Fig. 3).

Fig. 2 Root system of a 21-days-old maize plant (sample 1) grown in a slab-shaped rhizotron (150 × 150 × 15 mm). The roots were captured with neutron computed laminography, segmented and 3D-rendered from different perspectives using VG Studio Max 3.1. In the horizontal barrier layer with higher water content the contrast between roots and soil was lower and not all roots could be segmented. The pH optode is attached at the front, the oxygen optode at the back side of the rhizotron as illustrated in the video in the supplementary information
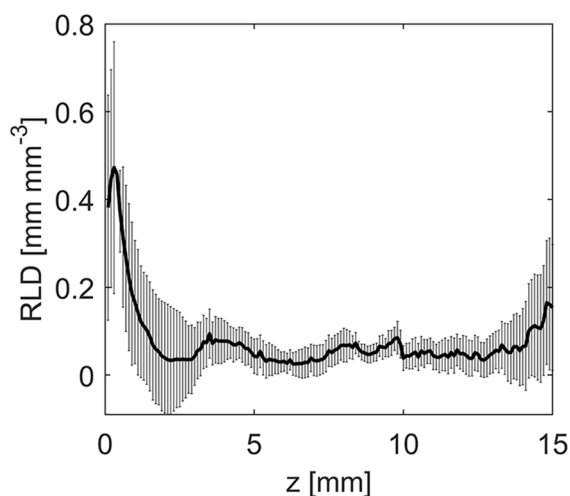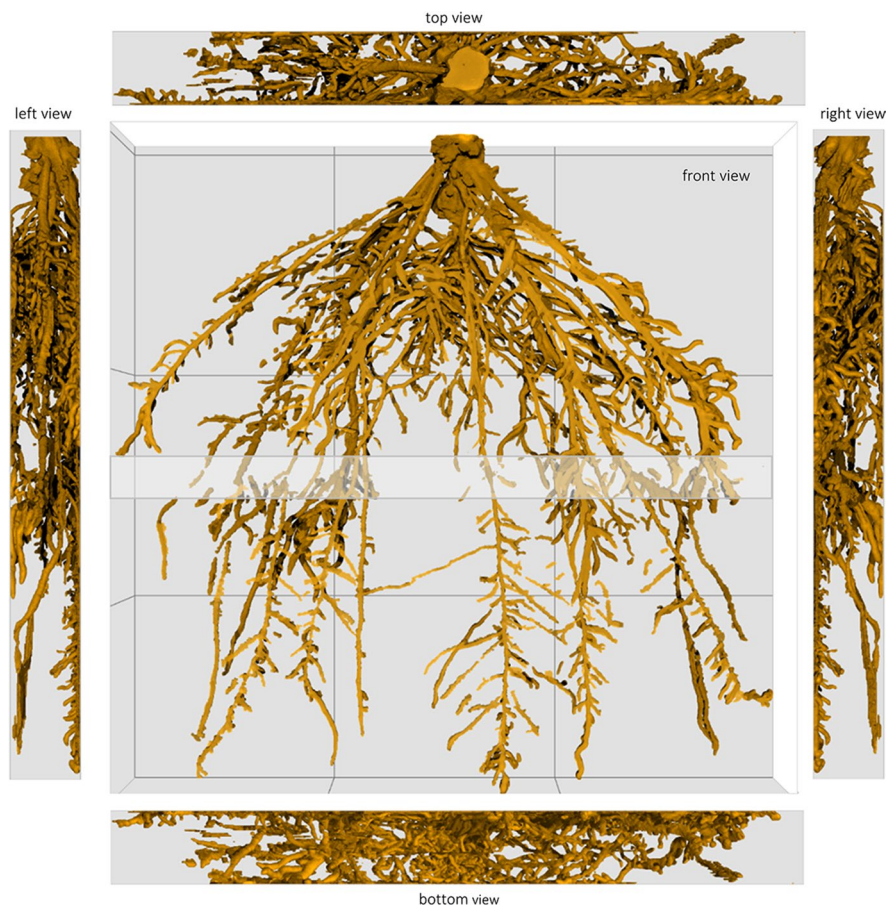

Fig. 3 Spatial distribution of the root length density (RLD, mm root length mm^{-3} soil) plotted in the thickness direction z of the rhizotrons (mean ± SD, n = 3). Positions of the pH and oxygen optode are z = 0 mm and z = 15 mm, respectively

The 3D root systems of the other two maize plants are shown in the supplementary information (Fig. S1).

Local impact of roots on the oxygen distribution pattern

We hypothesized that not only the roots growing in direct contact to the planar optode (located at z = 0 mm and z = 15 mm, Fig. 3), but also those parts of the root system located in greater distance to the sensor impact the measured oxygen and pH pattern, respectively. To test this, we projected different sub-volumes extracted from the 3D laminographic scan of the root system onto the 2D oxygen maps (Fig. 4). Starting with the roots growing directly along the optode (up to 0.1 mm distance), we successively included roots located within 1 mm up to 15 mm distance from the sensor (Fig. 5). The latter then includes all roots. Additionally, we compared oxygen concentration with respect to the distance to
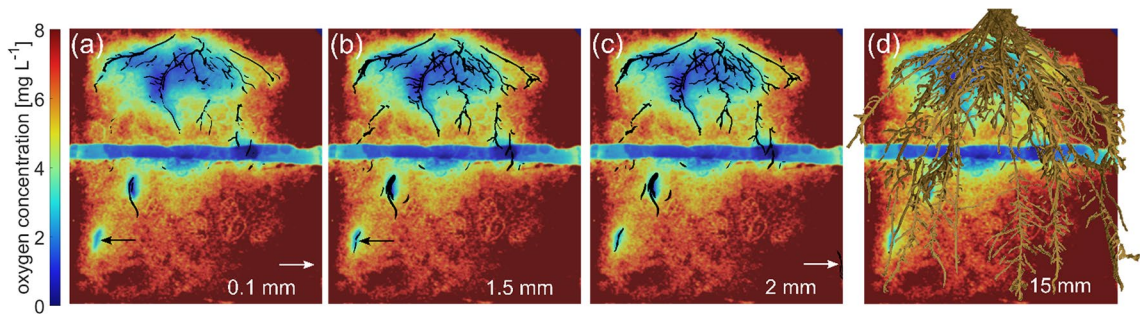
Fig. 4 Soil oxygen distribution at one side of maize sample 1, captured 2 h after watering overlaid with different sub-volumes of the root system: **a** 0.1 mm (roots growing directly along the O_2 optode); **b** 1.5 mm; **c** 2 mm and **d** 15 mm, i.e. the complete root system, shown in a perspective view from the opposite side. The black arrow in (**a**) marks a region where oxygen consumption of a root grown at a distance of about 1.5 mm is detected. In contrast, the white arrow in (**c**) shows a root segment at a distance of 2 mm, whose influence on the oxygen distribution is not visible yet. Oxygen consumption by this part of the root system could, however, be detected at 13 h after watering as shown in Fig. 5a)

the nearest root surface in 3D in the upper and lower compartment of the rhizotrons (Fig. 5 and Fig. S2).

Two hours after watering, local oxygen depletion zones formed around individual roots (Fig. 4a). Roots growing within a distance of up to 1.5 mm from the planar oxygen sensor had a substantial influence on the observed oxygen distribution (Fig. 4b). The oxygen uptake of roots located at a greater distance from the oxygen sensor was not yet detected at this time as indicated by the root segment grown at 2 mm distance (highlighted by a white arrow in Fig. 4c) and the steep oxygen gradient towards the root surface (Fig. 6).

The laminography revealed that not many roots grew directly along the oxygen optode in the lower part of the rhizotron (c.f. Figure 4a). However, 13 h after rewetting, regions of oxygen consumption started to form in the bottom part of the rhizotron as well (Fig. 5a). The depletion zones (O_2-conc. < 1.5 mg L^{-1}) can be attributed to metabolic activity of the roots located in the distance range of 7.5 mm from the optodes (Fig. 6a).

In the further course of the experiment (c.f. Figure 5c), different oxygen patterns formed above and below the barrier layer. A higher total root length (3640 mm vs. 2560 mm in the lower compartment) and evaporation in the upper part of the system resulted in a quicker decrease in soil moisture from 0.20 cm^3 cm^{-3} to 0.14 cm^3 cm^{-3} (c.f. Figure 5d) which lead to well aerated conditions in the upper soil compartment (c.f. Figure 5c and 6b). The roots in the lower compartment respired the available oxygen. The diffusive transport of oxygen from the ambient air was still limited by

the water-saturated barrier layer but likely not fully restricted (Fig. 5c, black arrow). Additionally, local oxygenation started at the bottom part which can be explained by sealing failure (Fig. 5c, black arrow), which is supported by the local change in water content (Fig. 5f). Further water uptake by the roots led to a steady reduction of the soil water content and promoted the re-aeration of the lower soil compartment (Fig. 5e and Fig. 6a). In contrast, oxygen concentration in the lower compartment of the other two maize plants remained < 1.5 mg L^{-1} 40 h after rewetting as re-aeration was still restricted (Fig. S2 a, c). The complementary measurement of 2D soil water maps (Fig. 5b, d and f) and 3D RSA, the latter revealing the distance between roots and detector, provided key information to understand the spatial and temporal distribution of oxygen concentration in this experiment.

Local impact of roots on the pH distribution pattern

Analogous to the evaluation of oxygen concentrations, the influence of the maize root system on the local soil pH was analyzed. The majority of the root system grew close to the pH optode (Fig. 3). Clear patterns of local acidification close to the roots growing within 2 mm distance to the pH sensor could be observed in the lower compartment of the rhizotron (c.f. Figure 7a–c). Some root segments also alkalinized their immediate environment. The difference in mean pH between top and bottom compartment (pH$_{mean,top}$ = 5.4; pH$_{mean,bottom}$ = 6.5) is a result of the non-uniform distribution of the root system featuring

Fig. 5 Time series of oxygen concentration for maize sample 1 are shown in (**a**, **c**, **e**) and soil water maps in (**b**, **d**, **f**), as measured in the maize root system by optical fluorescence and neutron imaging. Roots not further than 7.5 mm from the optode were projected onto the oxygen maps. The black arrows in (**c**) mark regions of commencing re-aeration

13 hours after watering

25 hours after watering

40 hours after watering
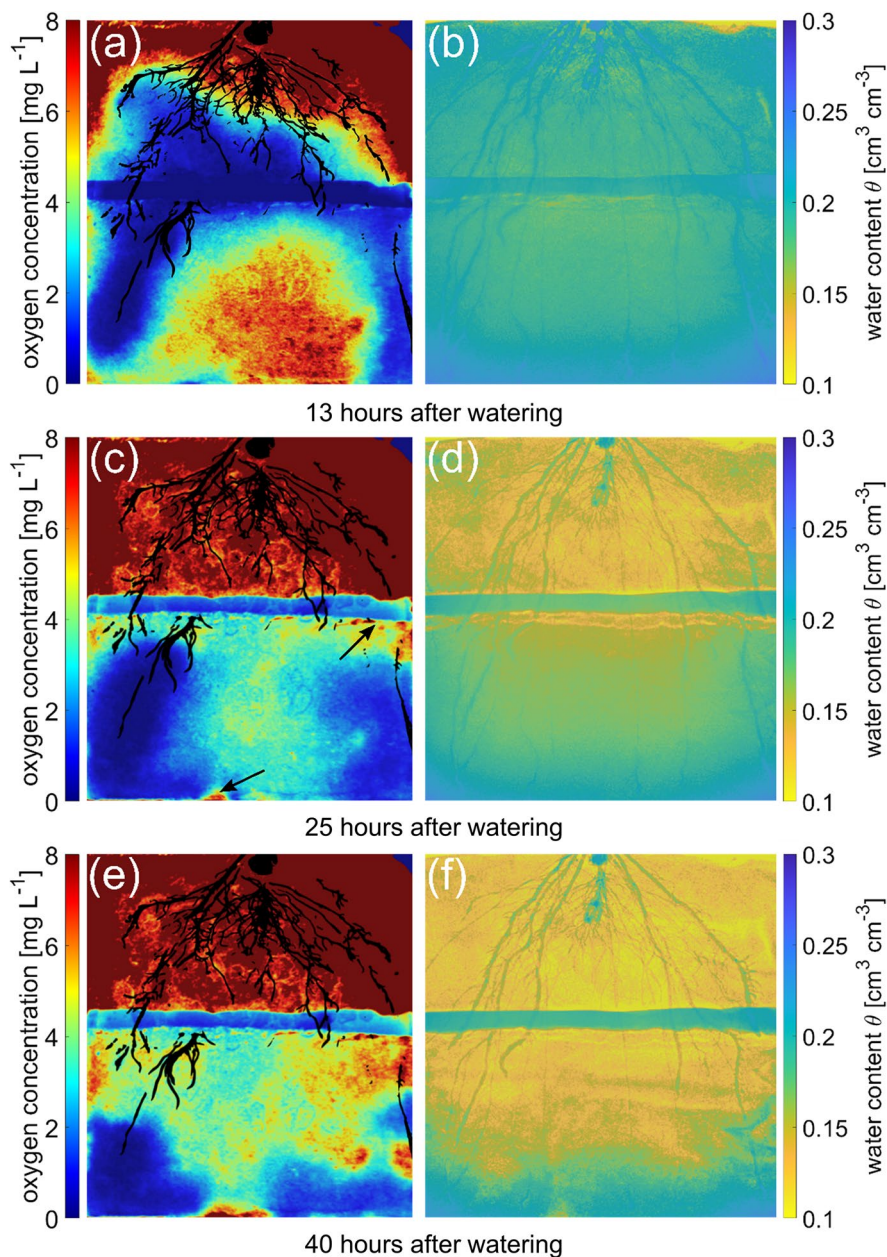
more roots in upper compartment (c.f. Figure 7d, day 5 after rewetting). The mean water content of the two compartments differed only marginally at this time (0.090 cm^3 cm^{-3} vs. 0.094 cm^3 cm^{-3}, not shown here). During the 6-day experiment the mean pH changed slightly from pH = 5.9 to pH = 5.5 in the upper compartment and from pH = 6.1 to pH = 6.5 in the lower compartment (Fig. S3). While the local patterns of pH change in the lower compartment can be attributed to single roots within 2 mm distance to

the sensor, there may also be an impact of the entire root system on mean pH changes. This highlights the importance to gain complementary information on 3D root distribution within the studied systems.

Discussion

Applying NCL, we succeeded to reproduce the three-dimensional structure of maize root systems in

Fig. 6 Oxygen concentration as a function of the Euclidean distance to the nearest root surface in 3D of maize sample 1 in the lower compartment (**a**) and the upper compartment (**b**). Line color indicates the time (in hours) after rewetting the samples from 0.1 cm^3 cm^{-3} to 0.24 cm^3 cm^{-3} volumetric water content
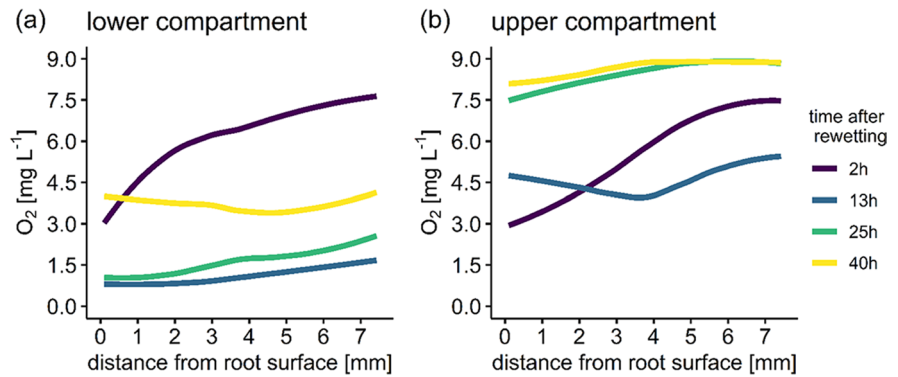
a quality appropriate to extract the 3D root system architecture. We found the majority of roots growing close to the pH optode at the front side of the container. Apparently, the hydrophilic properties of the pH sensor matrix, which is mainly composed of hydrogel, have favored root growth, probably due to the higher water availability. In contrast, the oxygen sensor matrix is composed of a hydrophobic polystyrene material and did not have an attracting effect on roots. However, some roots may accumulate there just as further growth in this direction is geometrically not possible. By image registration, we correlated the 3D information from NCL to the spatiotemporal pattern of soil oxygen concentration and pH changes derived by optical fluorescence imaging and complemented it with 2D water maps measured by neutron radiography. This way, the influence of roots on the measured pH and O$_2$ concentration maps could be evaluated, considering the actual root-sensor distance and the local soil water content. Knowledge of the local soil water content is a prerequisite because the oxygen

transport in the aqueous phase is substantially slower than in the gaseous phase. Though concentrations and transport of oxygen in soils has been investigated extensively, few studies describe oxygen dynamics on the rhizosphere scale (Ben-Noah and Friedman 2018). We observed that respiration of roots in direct contact to the oxygen sensor led to an immediate reduction of the local oxygen concentration. However, when water-saturated soil conditions prevailed for many hours the sensor also detected an oxygen consumption of roots at a greater distance, i.e. the respiration activity of the entire root system became evident over time. Local oxygen concentration and soil moisture can vary dynamically in the rhizosphere forming spatiotemporal patterns that depend on respiration activity of roots and microbes, on soil structure, irrigation and root growth (Cook et al. 2007; Watt et al. 2006). In this study, root respiration (including microbial oxygen consumption in the rhizosphere) resulted in oxygen deficiency especially in the lower compartment of the rhizotron where the
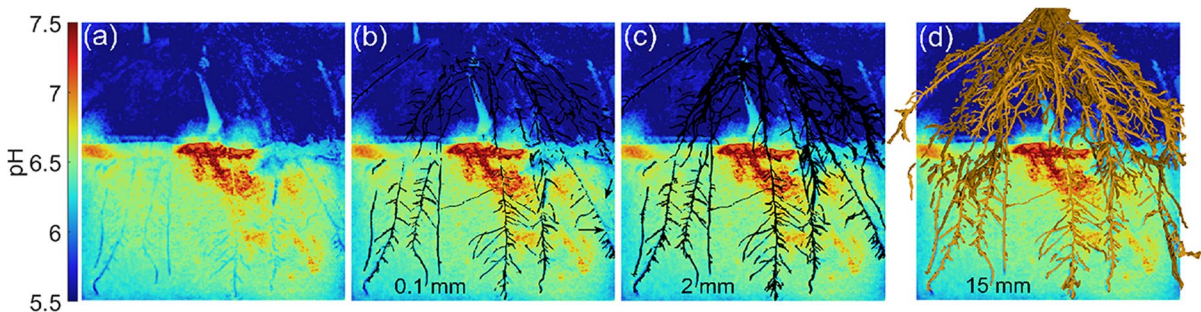
Fig. 7 **a** Soil pH distribution 5 days after watering (maize sample 1). Roots with increasing distance to the optode were projected onto the pH maps: **b** 0.1 mm (directly touching the

optode), **c** 2 mm, **d** 15 mm (all roots). The two black arrows in (**b**) mark positions where the observed pH pattern was affected by roots located within a distance of 0.1 mm to 2 mm

gas exchange with the atmosphere was restricted by the barrier layer. The formation of oxygen depletion zones was linked to the local root length density and the measured concentration gradients depended on the distance between root and sensor. This is in line with other studies measuring oxygen concentrations in the rhizosphere. Depending on the water content of the soil, the oxygen gradients around the roots extended over a distance of more than 4 mm into the soil (Kuzyakov and Razavi 2019).

Roots frequently excrete organic compounds stimulating microbial activity and strongly influencing the pH of rhizosphere. We found that roots in direct vicinity (up to 2 mm) to the pH optode caused a distinct rhizosphere pattern of reduced local soil pH, very likely by their exudations. Over the course of 6 days, we observed a slight acidification (0.4 pH units) in the upper compartment whereas the lower compartment shows a slight alkalization (0.4 pH units). It has been reported earlier that both alkalization and acidification could occur along single roots, which can be attributed to various root functions (Chaignon et al. 2002). Changes in physiological properties occur along the roots as a result of tissue aging and differentiation (Hodge et al. 2009). Jaillard et al. (1996) defined four areas of activity along the maize root and showed that the area next to the base of the stem, where second order roots emerge and elongate, strongly acidifies the environment. Additionally, the ability of plants to acidify or alkalize their rhizosphere depends on their environment. Chaignon et al. (2002) showed that tomato and oilseed rape decreased rhizosphere pH when growing under calcareous condition but alkalized the rhizosphere under acidic soil conditions. In summary, acidification and alkalization in the rhizosphere of plants are well documented and the rhizosphere extent (~ 2 mm) is in line with other studies (Blossfeld et al. 2013; Chaignon et al. 2002; Hinsinger et al. 2003; Taylor and Bloom 1998). Another possibility is optode signal drift caused by dye leaching or by changes in soil water content. However, in a former study we could show the stability of the pH optode by recalibrating the matrix after the experiment (Rudolph-Mohr et al. 2014). For other optodes sensitive to CO_2, which is pH active due to the concomitant formation of carbonic acid, it was shown that the volumetric water content very much influenced the amount of detected CO_2 (Holz et al. 2020). Due to the complexity and interdependence of

root-soil interactions, the combination of 2D and 3D in-situ imaging techniques applied to the same sample can provide valuable experimental datasets to answer those questions. Coupling of in-situ imaging experiments with the parametrization of models is the key for an enhanced understanding of the interactions and processes within the rhizosphere (Roose et al. 2016).

One key challenge of the analysis of tomographic data of root systems in soil is the segmentation of the root system, i.e. the classification whether a pixel belongs to the root or soil domain. In wet soil conditions, the distinction between root and soil is particularly difficult. For this reason, we applied NCL only at the end of the experiment, when the low soil water content provided the most favorable contrast between roots and soil. We used a semi-automated region-growing algorithm with manually set seed-points to segment the roots in the laminographic data set. This method requires a high level of user interaction, as also reported from segmentation of large and complex root systems from X-ray tomography (Flavel et al. 2012). The future challenge is to implement classification protocols for automatic segmentation and therefore higher throughput. Further improvements in the image quality would greatly facilitate the applicability of automated segmentation algorithms and quantitative analysis of the RSA. This requires optimization of the imaging conditions, e.g. measuring at lower soil water content, adaptation of reconstruction algorithms and the use of neutron imaging facilities with higher neutron beam intensity, such as the imaging station NeXT located at Institut Laue-Langevin (ILL), Grenoble/ France (Tengattini et al. 2020) and the future neutron tomography station ODIN located at European Spallation Source (ESS), Lund/ Sweden (Andersen et al. 2020). Neutron computed laminography as a 3D imaging method is potentially suitable for the quantification of root traits such as root diameter, root length density, branching angles, number of root tips and surface area. It is intrinsically not suitable for the dynamic quantification of soil moisture and root water uptake in 3D, as tilting the rotational axis may induce gravitational driven shifts in the soil water distribution including plant stress influencing its transpiration behavior. Furthermore, tilting of the rhizotron during the laminography scan could also affect the oxygen distribution and was therefore applied only at the final day of the experiment. Certainly, the method provides the opportunity of 3D investigation of

root systems grown in rectangular slabs, a set-up often used for optical imaging approaches.

Neutron computed laminography in combination with optical imaging of biogeochemical gradients is an important next step in understanding rhizosphere processes. The presented new combination of imaging methods facilitates systematical investigation of the influence of different environmental conditions on a wide range of dynamic processes in the rhizosphere. The method also allows in general for a three-dimensional investigation of root systems grown in laterally extended rhizoboxes, which has a wide range of applications in rhizosphere research.

Data availability The raw data and reconstructed 3D dataset from neutron computed laminography of one maize sample is available at the datacite repository from Helmholtz Centre Berlin under http://doi.org/10.5442/ND000004.

Declarations

Conflicts of interest The authors have no conflicts of interest to declare that are relevant to the content of this article.

References

Aguilar EA, Turner DW, Gibbs DJ, Armstrong W, Sivasithamparam K (2003) Oxygen distribution and movement, respiration and nutrient loading in banana roots (Musa spp. L.) subjected to aerated and oxygen-depleted environments. Plant Soil 253:91–102. https://doi.org/10.1023/A:1024598319404

Ahmed MA, Zarebanadkouki M, Meunier F, Javaux M, Kaestner A, Carminati A (2018) Root type matters: measurement of water uptake by seminal, crown, and lateral roots in maize. J Exp Bot 69:1199–1206. https://doi.org/10.1093/jxb/erx439

Andersen KH, Argyriou DN, Jackson AJ et al (2020) The instrument suite of the European Spallation Source. Nuclear Instrum Methods Phys Res Sect A 957:163402. https://doi.org/10.1016/j.nima.2020.163402

Aravena JE, Berli M, Ghezzehei TA, Tyler SW (2011) Effects of root-induced compaction on rhizosphere hydraulic properties—X-ray microtomography imaging and numerical simulations. Environ Sci Technol 45:425–431. https://doi.org/10.1021/es102566j

Ben-Noah I, Friedman SP (2018) Review and evaluation of root respiration and of natural and agricultural processes of soil aeration. Vadose Zone J 17:170119. https://doi.org/10.2136/vzj2017.06.0119

Blossfeld S, Schreiber CM, Liebsch G, Kuhn AJ, Hinsinger P (2013) Quantitative imaging of rhizosphere pH and CO2 dynamics with planar optodes. Ann Bot 112:267–276. https://doi.org/10.1093/aob/mct047

Chaignon V, Bedin F, Hinsinger P (2002) Copper bioavailability and rhizosphere pH changes as affected by nitrogen supply for tomato and oilseed rape cropped on an acidic and a calcareous soil. Plant Soil 243:219–228

Cook FJ, Knight JH, Kelliher FM (2007) Oxygen transport in soil and the vertical distribution of roots. Aust J Soil Res 45:101–110. https://doi.org/10.1071/SR06137

Dara A, Moradi BA, Vontobel P, Oswald SE (2015) Mapping compensating root water uptake in heterogeneous soil conditions via neutron radiography. Plant Soil 397:273–287. https://doi.org/10.1007/s11104-015-2613-3

Esser HG, Carminati A, Vontobel P, Lehmann EH, Oswald SE (2010) Neutron radiography and tomography of water distribution in the root zone. J Plant Nutr Soil Sci 173:757–764. https://doi.org/10.1002/jpln.200900188

Fisher SL, Holmes DJ, Jorgensen JS, Gajjar P, Behnsen J, Lionheart WRB, Withers PJ (2019) Laminography in the lab: imaging planar objects using a conventional X-ray CT scanner. Meas Sci Technol 30:035401. https://doi.org/10.1088/1361-6501/aafcae

Flavel RJ, Guppy CN, Tighe M, Watt M, McNeill A, Young IM (2012) Non-destructive quantification of cereal roots in soil using high-resolution X-ray tomography. J Exp Bot 63:2503–2511. https://doi.org/10.1093/jxb/err421

Haber-Pohlmeier S, Tötzke C, Lehmann E, Kardjilov N, Pohlmeier A, Oswald SE (2019) Combination of magnetic resonance imaging and neutron computed tomography for three-dimensional rhizosphere imaging. Vadose Zone J 18:180166. https://doi.org/10.2136/vzj2018.09.0166

Helfen L, Xu F, Schillinger B, Calzada E, Zanette I, Weitkamp T, Baumbach T (2011a) Neutron laminography-a novel approach to three-dimensional imaging of flat objects with neutrons. Nuclear Instrum Methods Phys Res Sect A 651:135–139. https://doi.org/10.1016/j.nima.2011.01.114

Helfen L, Myagotin A, Mikulík P, Pernot P, Voropaev A, Elyyan M, Di Michiel M, Baruchel J, Baumbach T (2011b) On the implementation of computed

laminography using synchrotron radiation. Rev Sci Instrum 82:063702. https://doi.org/10.1063/1.3596566

Hinsinger P, Plassard C, Tang CX, Jaillard B (2003) Origins of root-mediated pH changes in the rhizosphere and their responses to environmental constraints: a review. Plant Soil 248:43–59. https://doi.org/10.1023/A:1022371130939

Hinsinger P, Gobran GR, Gregory PJ, Wenzel WW (2005) Rhizosphere geometry and heterogeneity arising from root-mediated physical and chemical processes. New Phytol 168:293–303. https://doi.org/10.1111/j.1469-8137.2005.01512.x

Hinsinger P, Bengough AG, Vetterlein D, Young IM (2009) Rhizosphere: biophysics, biogeochemistry and ecological relevance. Plant Soil 321:117–152. https://doi.org/10.1007/s11104-008-9885-9

Hodge A, Berta G, Doussan C, Merchan F, Crespi M (2009) Plant root growth, architecture and function. Plant Soil 321:153–187. https://doi.org/10.1007/s11104-009-9929-9

Holz M, Becker JN, Daudin G, Oburger E (2020) Application of planar optodes to measure CO2 gradients in the rhizosphere of unsaturated soils. Rhizosphere 16:100266. https://doi.org/10.1016/j.rhisph.2020.100266

Jaillard B, Ruiz L, Arvieu JC (1996) pH mapping in transparent gel using color indicator videodensitometry. Plant Soil 183:85–95. https://doi.org/10.1007/BF02185568

Kardjilov N, Hilger A, Manke I, Woracek R, Banhart J (2016) CONRAD-2: the new neutron imaging instrument at the Helmholtz-Zentrum Berlin. J Appl Crystallogr 49:195–202. https://doi.org/10.3139/120.111261

Koebernick N, Daly KR, Keyes SD, George TS, Brown LK, Raffan A, Cooper LJ, Naveed M, Bengough AG, Sinclair I, Hallett PD, Roose T (2017) High-resolution synchrotron imaging shows that root hairs influence rhizosphere soil structure formation. New Phytol 216:124–135. https://doi.org/10.1111/nph.14705

Kuzyakov Y, Razavi BS (2019) Rhizosphere size and shape: temporal dynamics and spatial stationary. Soil Biol Biochem 135:343–360. https://doi.org/10.1016/j.soilbio.2019.05.011

Menon M, Robinson B, Oswald SE, Kaestner A, Abbaspour KC, Lehmann E, Schulin R (2007) Visualization of root growth in heterogeneously contaminated soil using neutron radiography. Eur J Soil Sci 58:802–810. https://doi.org/10.1111/j.1365-2389.2006.00870.x

Moradi AB, Conesa HM, Robinson B, Lehmann E, Kuehne G, Kaestner A, Oswald S, Schulin R (2009) Neutron radiography as a tool for revealing root development in soil: capabilities and limitations. Plant Soil 318:243–255. https://doi.org/10.1007/s11104-008-9834-7

Moradi AB, Carminati A, Vetterlein D, Vontobel P, Lehmann E, Weller U, Hopmans JW, Vogel H-J, Oswald SE (2011) Three-dimensional visualization and quantification of water content in the rhizosphere. New Phytol 192:653–663. https://doi.org/10.1111/j.1469-8137.2011.03826.x

Pohlmeier A, Oros-Peusquens A, Javaux M, Menzel MI, Vanderborght J, Kaffanke J, Romanzetti S, Lindenmair J, Vereecken H, Shah NJ (2008) Changes in soil water content resulting from Ricinus root uptake monitored by magnetic resonance imaging. Vadose Zone J 7:1010–1017. https://doi.org/10.2136/vzj2007.0110

Roose T, Keyes SD, Daly KR, Carminati A, Otten W, Vetterlein D, Peth S (2016) Challenges in imaging and predictive modeling of rhizosphere processes. Plant Soil 407:9–38. https://doi.org/10.1007/s11104-016-2872-7

Rudolph N, Esser HG, Carminati A, Moradi AB, Hilger A, Kardjilov N, Nagl S, Oswald SE (2012) Dynamic oxygen mapping in the root zone by fluorescence dye imaging combined with neutron radiography. J Soil Sediments 12:63–74. https://doi.org/10.1007/s11368-011-0407-7

Rudolph N, Voss S, Moradi AB, Nagl S, Oswald SE (2013) Spatio-temporal mapping of local soil pH changes induced by roots of lupin and soft-rush. Plant Soil 369:669–680. https://doi.org/10.1007/s11104-013-1775-0

Rudolph-Mohr N, Vontobel P, Oswald SE (2014) A multi-imaging approach to study the root-soil interface. Ann Bot 114:1779–1787. https://doi.org/10.1093/aob/mcu200

Rudolph-Mohr N, Totzke C, Kardjilov N, Oswald SE (2017) Mapping water, oxygen, and pH dynamics in the rhizosphere of young maize roots. J Plant Nutr Soil Sci 180:336–346. https://doi.org/10.1002/jpln.201600120

Salvemini F, Grazzi F, Kardjilov N, Manke I, Civita F, Zoppi M (2015) Neutron computed laminography on ancient metal artefacts. Anal Methods 7:271–278. https://doi.org/10.1039/C4AY02014F

Smith S, Smet De, Ive. (2012) Root system architecture: insights from Arabidopsis and cereal crops. Phil Trans R Soc B 367:1441–1452. https://doi.org/10.1098/rstb.2011.0234

Strömberg N (2008) Determination of ammonium turnover and flow patterns close to roots using Imaging optodes. Environ Sci Technol 42:1630–1637. https://doi.org/10.1021/es071400q

Taylor AR, Bloom AJ (1998) Ammonium, nitrate, and proton fluxes along the maize root. Plant Cell Environ 21:1255–1263. https://doi.org/10.1046/j.1365-3040.1998.00357.x

Tengattini A, Lenoir N, Andò E, Giroud B, Atkins D, Beaucour J, Viggiani G (2020) NeXT-Grenoble, the neutron and X-ray tomograph in Grenoble. Nuclear Instrum Methods Phys Res Sect A 968:163939. https://doi.org/10.1016/j.nima.2020.163939

Tötzke C, Kardjilov N, Manke I, Oswald SE (2017) Capturing 3D water flow in rooted soil by ultra-fast neutron tomography. Sci Rep 7:6192. https://doi.org/10.1038/s41598-017-06046-w

Tötzke C, Kardjilov N, Lenoir N, Manke I, Oswald SE, Tengattini A (2019) What comes next?—high-speed neutron tomography at ILL. Opt Express 27:28640–28648. https://doi.org/10.1364/OE.27.028640

Tötzke C, Kardjilov N, Hilger A, Rudolph-Mohr N, Manke I, Oswald SE (2021) Three-dimensional in vivo analysis of water uptake and translocation in maize roots by fast neutron tomography. Sci Rep 11:10578. https://doi.org/10.1038/s41598-021-90062-4

van Dusschoten D, Metzner R, Kochs J, Postma JA, Pflugfelder D, Bühler J, Schurr U, Jahnke S (2016) Quantitative 3D analysis of plant roots growing in soil using magnetic resonance imaging. Plant Physiol 170:1176–1188. https://doi.org/10.1104/pp.15.01388

Watt M, Silk WK, Passioura JB (2006) Rates of root and organism growth, soil conditions, and temporal and spatial

development of the rhizosphere. Ann Bot 97:839–855. https://doi.org/10.1093/aob/mcl028